THE JOURNAL OF PHYSICAL CHEMISTRY C
A JOURNAL OF THE AMERICAN CHEMICAL SOCIETY

pubs.acs.org/JPCC

Article

Simulated Interstellar Photolysis of N_2O Ice: Selectivity in Photoproducts

Published as part of The Journal of Physical Chemistry C specialissue "Heterogeneous Drivers of Ice Formation".

Bijesh K. Malla, Soham Chowdhury, Devansh Paliwal, Hanoona K. M., Gaurav Vishwakarma, Rabin Rajan J. Methikkalam, and Thalappil Pradeep*

Cite This: https://doi.org/10.1021/acs.jpcc.4c06624

Read Online

ACCESS | Metrics & More | Article Recommendations | Supporting Information

ABSTRACT: Thermal diffusion and recombination control the kinetics of photochemical reactions of reactive radicals formed by ultraviolet photon irradiation in interstellar ices. Here, we show that upon vacuum ultraviolet photolysis, N_2O ice produces O_3 and several oxides of nitrogen, such as NO, NO_2, N_2O_2, N_2O_3, N_2O_4, and N_2O_5 in interstellar ice mimics. Photoproducts within the bulk and on the surface were analyzed using reflection absorption infrared spectroscopy and Cs^+ ion-based secondary ion mass spectrometry, while desorbed species were studied using temperature-programmed desorption mass spectrometry. Notably, thermal annealing of the photoirradiated ice to 90 K resulted in a significant increase in NO and N_2O_3. Photoirradiation at 10 K revealed the dominance of three atom photoproducts, such as NO_2 and O_3. In contrast, irradiation at 50 K significantly enhanced the production of four or higher atom photoproducts (N_2O_2, N_2O_3, N_2O_4, and N_2O_5). This behavior is attributed to the restricted diffusion of reactive radicals and unstable oxygen species (O and O_3) at 10 K, which confines radical−radical reactions to three or fewer atom photoproducts, whereas higher temperatures facilitate oxygen and other radical diffusion and recombination, yielding heavier photoproducts. These results throw light on the thermal diffusion effects on the kinetics of photoproducts in interstellar ice mimics.

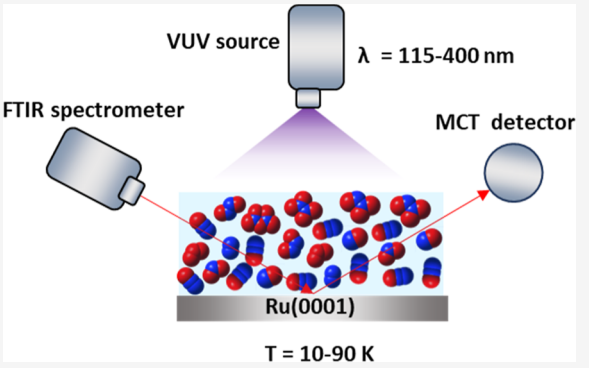

INTRODUCTION

The photochemistry of the molecular ices present in the interstellar medium (ISM) plays a significant role in forming complex organic molecules.[1] More than 300 molecules, including neutrals, ions, and radicals, have been identified in ISM.[2] Bigger molecules such as C_{60}, C_{70}, and polyaromatic hydrocarbons raise questions about their formation mechanisms in cold conditions.[3] Molecules, dust grains, and atoms in the ISM are continuously exposed to ultraviolet (UV) photons from nearby stars and other sources, leading to photochemical reactions. These processes produce complex molecular species, including organic compounds essential to the emergence of life.[4] Laboratory experiments involving the irradiation of molecular ices in simulated interstellar conditions with charged particles (ions and electrons) and UV photons have revealed the synthesis of amino acids and nucleobases, which is crucial for understanding the origins of biology.[1,5,6] In such reactions, diffusion of reactive intermediates plays a critical role in determining reaction kinetics. When radicals are properly oriented, and the reaction is barrierless, it is expected to proceed efficiently. If the diffusion barriers are significantly higher than the reaction barriers, reactants are likely to remain adsorbed next to each other until the reaction occurs.[7,8] Although the photochemistry of various molecules has been reported in interstellar ice analogs, a crucial gap in our understanding is the diffusion behavior of different radicals within ice matrices.[7,9−16] Specifically, how thermal and nonthermal diffusion occurs across various ices at different temperatures is not well understood.[1]

N_2O was first detected in the gas phase within the molecular cloud Sgr B2(M) in 1994.[17] Recently, the James Webb Space Telescope (JWST) has identified N_2O in the condensed phase within protostellar systems.[18] N_2O plays a major role in the dissociation of ozone in our stratosphere.[19] However, when N_2O was subjected to electron irradiation at very low temperatures (25 K), it produced ozone in the solid phase.[20] In the ISM, oxygen, and nitrogen are the major elements in molecular clouds and star-forming regions.[21−23] Despite their ubiquity, only six molecules: nitrous oxide (N_2O),[17] nitroxyl

Received: September 30, 2024
Revised: December 7, 2024
Accepted: December 12, 2024

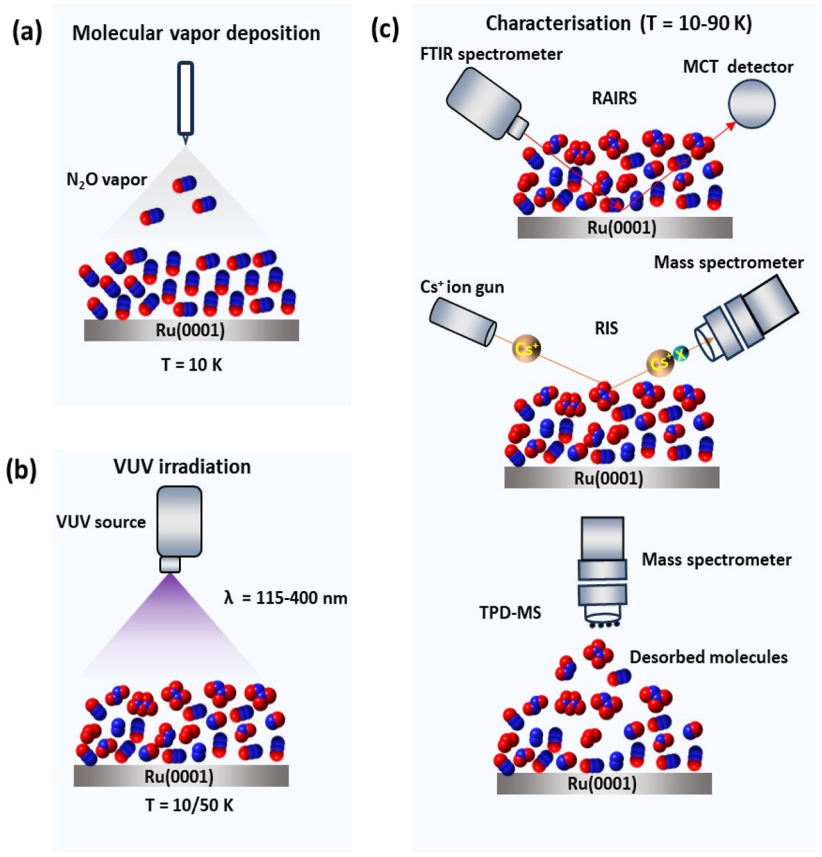

Figure 1. Schematic presentation of experimental protocols used in this study. (a) 150 ML of N_2O ice was created on Ru(0001) substrate by molecular vapor deposition at 10 K. (b) N_2O ice was irradiated with VUV photon by using deuterium lamp. (c) Photoirradiated ice was characterized by RAIRS, RIS, and TPD-MS.

(HNO),[24,25] nitrous acid (HONO),[26] fulminic acid (HCNO),[27] nitric oxide (NO),[28] and hydroxylamine (NH_2OH)[29] containing N−O bond have been identified in the interstellar and circumstellar medium.

Under laboratory interstellar medium (ISM) conditions, Jamieson et al. investigated the formation of N_2O by irradiating N_2 and CO ice at 10 K with 5 keV electrons,[30] where Halfen et al. studied the gas phase formation mechanism of N_2O by radical−radical reaction.[31] Sivaraman et al. demonstrated the formation of various N−O bond-bearing molecules by irradiating N_2O ice with 1 keV electron at 25 K.[20] Several studies also exist on the radiolysis of N_2O by bombarding fast ions ($^{14}N^+$),[32] and ($^{136}Xe^{23+}$). No report exists on the vacuum ultraviolet (VUV) photolysis of N_2O ice in ISM-simulated conditions. Also, there is a lack of understanding of the diffusion and recombination of radicals in different thermal conditions. In our previous study,[7] we demonstrated how nonthermal radical diffusion in highly and less ordered methyl chloride crystalline ice contributed to the formation of photoproducts. The present study focuses on the thermal diffusion of radicals in photoirradiated N_2O ice. In it, we have shown the VUV photolysis of pure N_2O ice under interstellar laboratory conditions, resulting in the formation of various N−O bearing molecules along with O_3. Photoirradiation experiments conducted at both 10 and 50 K reveal distinct, temperature-dependent distributions of photoproducts. Higher temperatures play a crucial role in reducing the thermal diffusion barrier for oxygen allotropes and reactive radicals, facilitating further recombination with nitrous oxides to form secondary photoproducts at higher temperatures. This suggests that varying temperature conditions could significantly influence the chemistry and composition of interstellar ices, providing valuable insights into the complex mechanisms underlying molecular evolution in space.

EXPERIMENTAL SECTION

Experimental Setup. The experiments were conducted within an ultrahigh vacuum (UHV) instrument, extensively described in our previous study.[33−35] The instrument is equipped with various analytical techniques, including reflection absorption infrared spectroscopy (RAIRS), low energy ion scattering (LEIS), temperature-programmed desorption (TPD) mass spectrometry, Cs^+ ion-based secondary ion mass spectrometry (SIMS), and a VUV lamp. To maintain a base pressure of 5×10^{-10} mbar, six turbomolecular pumps are attached to the chambers backed by multiple oil-free diaphragm pumps. Chamber pressure is monitored using a Bayard-Alpert gauge, regulated by a Maxi Gauge vacuum gauge controller (Pfeiffer, Model TPG 256 A).

To create a thin film of ice, a finely polished Ru(0001) crystal was used as the substrate, which was attached to a copper holder. The assembly can be cooled to 8 K by connecting it to a helium cryostat (ColdEdge technology). The substrate assembly can be heated to 1000 K using a resistive heater (25 Ω), which was used to control the temperature. An accurate ±0.5 K thermocouple sensor was used to detect the temperature of the substrate. Before each vapor deposition experiment, the substrate was repeatedly heated to a higher

https://doi.org/10.1021/acs.jpcc.4c06624
J. Phys. Chem. C XXXX, XXX, XXX−XXX

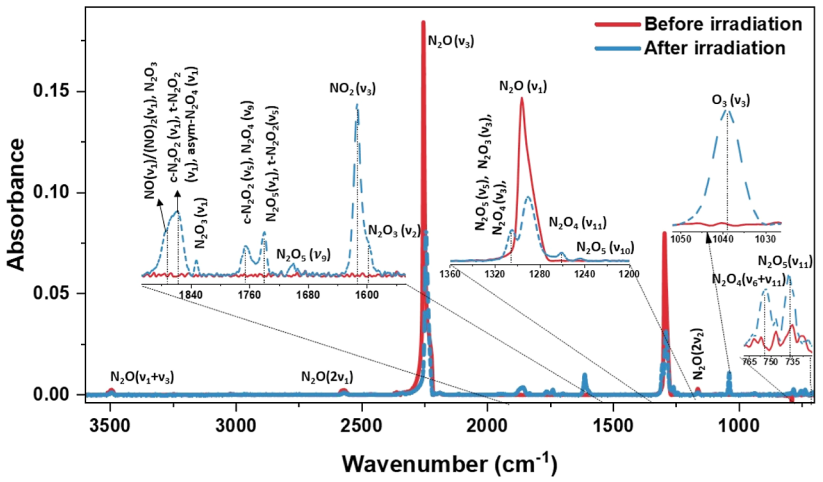

Figure 2. RAIR spectra of 150 ML of N_2O ice before and after 2 h VUV photoirradiation at 10 K in the mid-infrared region.

temperature to ensure a clean surface. It is important to note that the surface has only a minor influence on the current investigation, as our sample is a multilayer.

RAIRS AND TPD-MS SETUP

Reflection−absorption infrared (RAIR) data was collected using a Bruker FT-IR spectrometer (Vertex 70 model), covering the 4000−550 cm^{-1} range and with a spectral resolution of 2 cm^{-1}. The IR beam was directed onto the ice sample using a ZnSe viewport to get an incidence angle of 80 ± 7°. The reflected IR beam from the sample was analyzed by a liquid nitrogen-cooled mercury cadmium telluride (MCT) detector (Figure 1c). Dry N_2 was purged in the FTIR spectrometer, path of the IR radiation (outside UHV), and MCT detector compartment to reduce absorption by ambient moisture. An average of 512 scans was used to create each RAIR spectrum, which improved the signal-to-noise ratio. An Extrel quadrupole mass spectrometer was used for temperature-programmed desorption mass spectrometry (TPD-MS) in an out-of-sight configuration.

VUV Source. A deuterium lamp (30 W) of VUV emission range of 115−400 nm with a spectral bandwidth of 0.8 nm (shown in Figure S1) was employed as the UV light source. The VUV lamp was differentially pumped and attached to the UHV chamber through the MgF_2 window [with a cutoff at ∼114 nm (10.87 eV)]. This configuration allows the lamp to emit light at wavelengths as short as 115 nm effectively. The photon flux was measured to be approximately ∼6 × 10^{12} photons cm^{-2} s^{-1}.[7,36]

SIMS SETUP

The Cs^+ ion-based SIMS technique enables molecular identification and monitoring of surface reactions.[37] Cs^+ (m/z = 133) was selected for ion scattering due to their high depth resolution of approximately 1 bilayer and their capacity to detect neutral molecules on the N_2O ice surface.[38] Reactive ion scattering (RIS) experiment was performed using Cs^+ ions with a kinetic energy of 60 eV. The Cs^+ ion collides on the ice surface, forms adducts with neutral molecules on the surface, and drags them from the surface along its outgoing trajectory, a process known as the RIS (Figure 1c). The Cs^+ ion adducts with the neutral molecules are driven by an ion-neutral dipole interaction.[39] The mass of the Cs^+ ion adduct was determined with a quadrupole mass analyzer. To identify the mass of neutral photolysis products formed on the N_2O ice, the mass of Cs^+ (m/z = 133) is subtracted from the mass of the Cs^+ ion adduct.

Material and Sample Preparation. As received, nitrous oxide (N_2O) (Indogas, 99.9% purity) was connected to the main chamber through sample inlet lines controlled by high-precision metal leak valves. 150 ML of N_2O ice was prepared by vapor deposition on Ru(0001) at 10 K (Figure 1a). The vapor deposition coverage in the case of N_2 (ion gauge sensitivity factor was taken as 1) was expressed in monolayers (ML), assuming 1.33 × 10^{-6} mbar exposure in 1 s is equal to 1 ML, which was estimated to contain ∼1.1 × 10^{15} molecules cm^{-2}, as adopted in other reports.[40−42] To deposit 150 ML of N_2O ice, The chamber was backfilled with N_2O (ion gauge sensitivity factor −1.2) vapor at 5 × 10^{-7} mbar pressure for 5 min. The vacuum gauge was calibrated with nitrogen, and N_2O coverage may differ slightly in view of this uncorrected pressure reading. Mass spectra were taken simultaneously during vapor deposition to check the purity and ratio of the deposited molecules.

RESULTS AND DISCUSSION

Photochemistry of N_2O Ice. About 150 ML of amorphous ice thin film was prepared by depositing N_2O vapor on Ru(0001) substrate at 10 K. Figure S2 shows the RAIR spectrum of pure N_2O ice at 10 K, where N_2O is identified by different peaks; 3495 cm^{-1} ($\nu_1 + \nu_3$), 2575 ($2\nu_1$), 2554 (ν_3), 1296 (ν_1), 1164 ($2\nu_2$), 591 (ν_2) cm^{-1}. Following deposition, the sample was exposed to VUV photoirradiation for 2 h, and the resulting RAIR spectra were recorded (Figure 2). All the photoproducts were identified by their distinct infrared bands, consistent with the previous reports.[20,30,32,43−48] N_2O_3 is characterized by the peaks at 1863 (N−O stretch), 1832 (ν_1), 1594 (ν_2), and 1304 (ν_3) cm^{-1}. Both cis(c)-N_2O_2, and trans(t)-N_2O_2 are identified by the peaks 1855 (ν_1), 1765 (ν_5), 1742 (ν_5) cm^{-1}, N_2O_5 exhibits peaks at 1702 (ν_9), 1742 (ν_1) and 736 (ν_{11}) cm^{-1}, while N_2O_4 is characterized by 1260 (ν_{11}) and 753 ($\nu_6 + \nu_{11}$) cm^{-1}. O_3 is identified by the peak at 1039 cm^{-1} (ν_3), and NO and $(NO)_2$ is identified by the 1863−1874 cm^{-1} (ν_1) stretch.

After 2 h of irradiation at 10 K, seven major photo products-NO, NO_2, O_3, N_2O_2, N_2O_4, N_2O_3, and N_2O_5 were observed in the RAIR spectra. It is worth noting that O_2 and N_2, which are also major products of photoirradiation, cannot be identified

https://doi.org/10.1021/acs.jpcc.4c06624
J. Phys. Chem. C XXXX, XXX, XXX−XXX

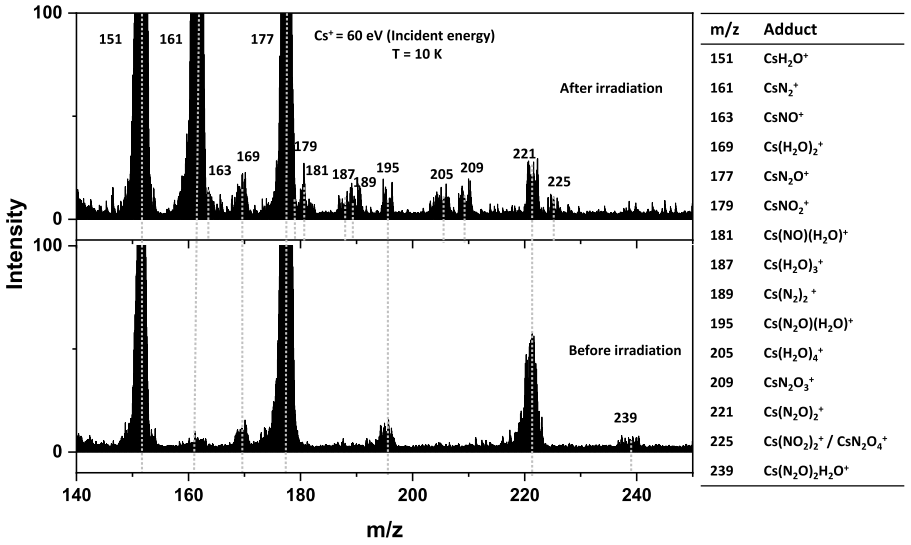

Figure 3. RIS mass spectra obtained after 60 min of VUV irradiation of amorphous N_2O ice. Mass spectrum of the irradiated ice was obtained by colliding the sample with 60 eV Cs^+ ions at 10 K. All the RIS photoproducts have been assigned, as listed in the table on the right.

by IR spectroscopy. The dissociation of N_2O primarily follows two pathways: in the first pathway, N_2O dissociates to N_2 molecules and atomic oxygens (1), and in the second pathway, it produces NO and N radicals (2).[49] The dissociation energy of the bond N═N (4.93 eV) is higher than that of N═O (1.68 eV),[50] making the first dissociation pathway more favorable, resulting in a high concentration of N_2 and O radicals.

$$N_2O + h\nu \rightarrow N_2 + O \quad (1)$$

$$\rightarrow NO + N \quad (2)$$

Another dissociation channel of N_2O is possible with the recombination of oxygen atoms, resulting in the formation of either two NO (3) or nitrogen and oxygen molecules (4).[32] Among these four reaction channels, it can be understood that NO is the other most abundantly produced molecule.

$$N_2O + O \rightarrow NO + NO \quad (3)$$

$$\rightarrow N_2 + O_2 \quad (4)$$

Further, high reactive oxygen radicals combine to form oxygen molecules (5), which can then combine with another oxygen radical to form ozone molecules (6).[20,32] During this process, N_2 absorbs an excess amount of energy.[51] The second most abundant product is nitrogen dioxide, formed by the recombination of NO and oxygen radicals (7).[52]

$$O + O \rightarrow O_2 \quad (5)$$

$$O_2 + O + N_2 \rightarrow O_3 + N_2 \quad (6)$$

$$NO + O \rightarrow NO_2 \quad (7)$$

Higher nitrous oxide can be formed with the recombination of N_2O with the diffused O_2 (8, 9), O_3 (10) inside the ice matrix.[32]

$$N_2O + O_2 \rightarrow N_2O_3 \quad (8)$$

$$N_2O + O_3 \rightarrow N_2O_4 \quad (9)$$

$$N_2O + 2O_2 \rightarrow N_2O_5 \quad (10)$$

Further recombination of primarily produced radicals (NO and O) and reactive molecules (NO_2, O_3) generates heavier molecules through the reaction pathways outlined below.[20,32,45,52]

$$NO + NO \rightarrow N_2O_2 \quad (11)$$

$$NO_2 + NO \rightarrow N_2O_3 \quad (12)$$

$$2NO_2 \rightarrow N_2O_4 \quad (13)$$

$$2NO_2 + O_3 \rightarrow N_2O_5 + O_2 \quad (14)$$

From the above reaction mechanism, it is well understood that primary photodissociation and association lead to the formation of small molecules with 2 to 3 atoms, such as NO, O_3, NO_2, O_2, N_2, etc. Further recombination of these molecules and radicals produces larger molecules like N_2O_3, N_2O_2, N_2O_4, and N_2O_5. Here, O is the smallest reactive species and can diffuse much faster than O_2 and O_3, so the reaction path 3 can more sufficiently occur relative to paths 8, 9, and 10 at very low temperatures.

The evolution of RAIR spectra of N_2O and photoproducts with respect to irradiation time (from 0 to 4 h) are shown in Figure S3. We considered the major infrared band for each molecule, calculated the band area, and plotted it in Figure S4. It was observed that all the photoproducts exhibited a sigmoidal growth pattern. The formation of NO_2 and O_3 increased until 150 min and then began to saturate, as these are primary radical associations. In contrast, *c*/*t*-N_2O_2, N_2O_4, N_2O_3, and N_2O_5 concentrations were saturated only after 90 min. The reaction mechanism reveals that the earlier photoproducts, NO_2 and O_3, are formed by recombining NO with O, and O_2 species. Other photo products emerge from secondary photo processes, which require additional radical recombination reactions. These secondary processes may be hindered by the limited diffusion of oxygen within the ice matrix at 10 K. This reduced mobility could explain why the formation of secondary photoproducts saturates within 90 min. The concentration of three or fewer atom photoproducts keeps increasing until 150 min due to the availability of O and NO radicals in close proximity. It is worth noting that although

https://doi.org/10.1021/acs.jpcc.4c06624
J. Phys. Chem. C XXXX, XXX, XXX−XXX

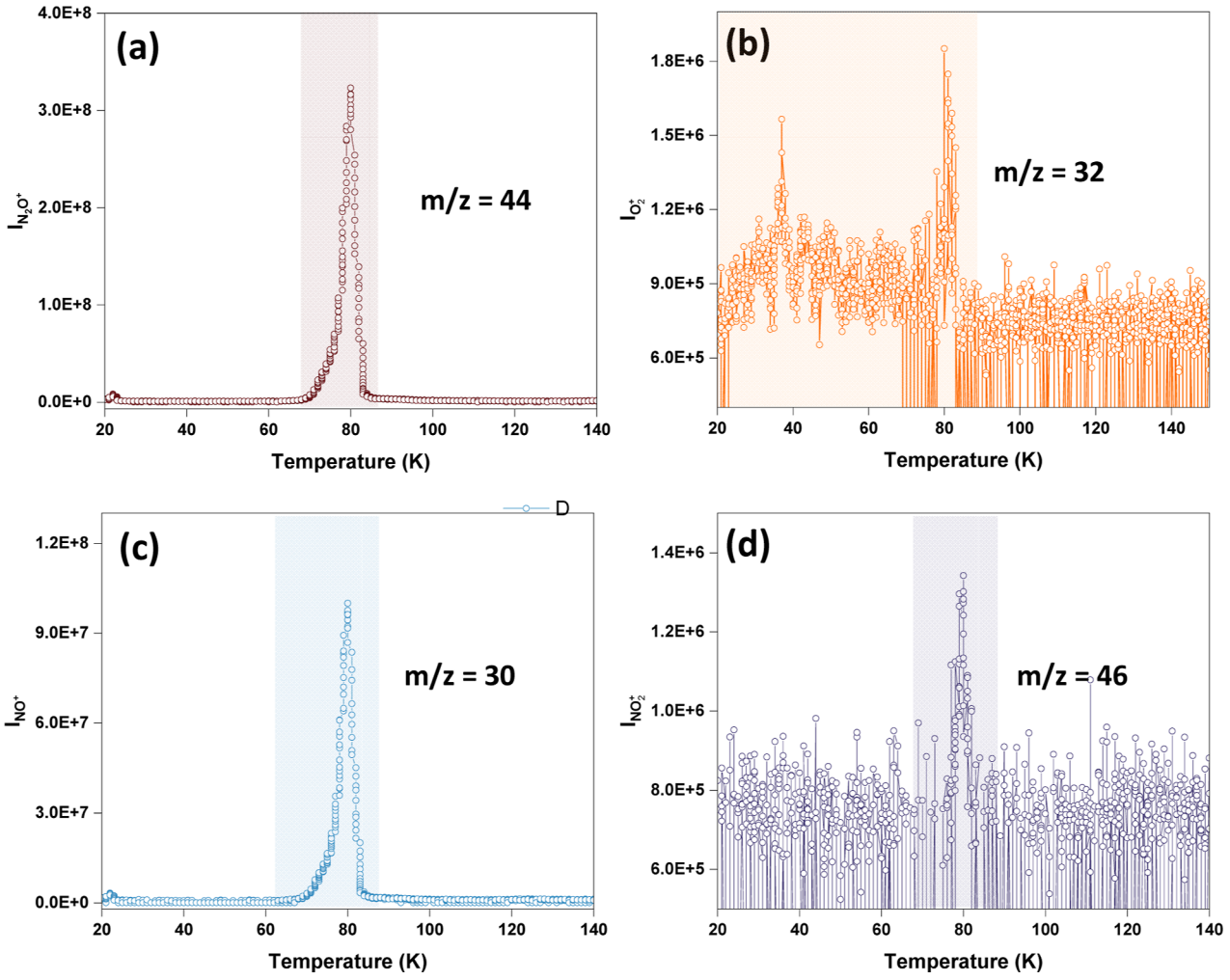

Figure 4. TPD-MS spectra of photo irradiated 150 ML of N_2O ice. Sublimation profiles using integrated ion counts at (a) m/z = 44, in (b) m/z = 32, in (c) m/z = 30 and (d) m/z = 46 are plotted.

photoinduced electrons may participate in this photochemistry, their impact is likely to be minimal due to multilayer ice, as electron penetration is confined to a depth of only 2 to 5 ML.[53−56]

While RAIRS primarily analyses the bulk properties of the ice film, SIMS is capable of probing the topmost monolayer of the ice. To study the surface photochemistry, we irradiated N_2O ice for 1 h and subsequently used SIMS to analyze the photoirradiated surface, identifying the molecules present on the surface. RIS with Cs^+ was employed, wherein Cs^+ ions form ionic clusters with neutral molecules on the ice surface, which are subsequently accelerated to the quadrupole mass spectrometer. Figure 3 shows the RIS spectra before and after irradiation. Before photoirradiation, five molecular cluster ion peaks were observed: m/z = 151 (CsH_2O^+), m/z = 169 [$Cs(H_2O)_2^+$], m/z = 179 (CsN_2O^+), m/z = 195 [$Cs(H_2O)(N_2O)^+$], m/z = 221 [$Cs(N_2O)_2^+$], and m/z = 239 [$Cs(N_2O)_2(H_2O)^+$]. Here, we note that the mass peaks for water molecules are attributed to the background deposition of water at 10 K during the experiment. Although the residual water was present only in trace amounts and did not significantly affect the photochemistry, the high dipole moment of H_2O resulted in high peak intensity for water in the RIS analysis. The extreme surface sensitivity of Cs^+ scattering is another reason for its high intensity.

After 1 h of irradiation, five new peaks emerged, corresponding to the Cs^+ adducts of N_2 (m/z = 161 and 189), NO (m/z = 163), NO + H_2O (m/z = 181), N_2O_3 (m/z = 209), and $(N_2O)_2/N_2O_4$ (m/z = 225). We did not observe any peaks for N_2O_5 and N_2O_2. Among the photoproducts, the intensity was generally low except for N_2, which suggests that reaction pathway 1 is the major dissociation channel that was not observed by IR spectroscopy. Here, we note that only 1 h irradiation was carried out to avoid more residual deposition of water, which can potentially affect the experiment.

For further evaluation, we conducted a temperature-programmed desorption mass spectrometry (TPD-MS) study of photoirradiated N_2O. In this experiment, N_2O was irradiated for 2 h at 10 K, followed by annealing of the photoproduced ice mixture up to 200 K at a rate of 10 K/min, while monitoring the m/z values of 44, 32, 30, and 46 (Figure 4). This allows us to understand how molecules form in the solid phase and transition to the gas phase during warming. We assigned m/z 44 to N_2O, which desorbs ∼80 K, consistent with its typical desorption temperature (Figure S5). The m/z 32 signal was attributed to O_3, with contributions from O_2. The desorption of O_3/O_2 started at 20 K and was completed at 80 K. This extended desorption range can be explained by the dissociation of O_3 and the formation of O_2 during thermal annealing, which has a lower desorption temperature. The m/z

https://doi.org/10.1021/acs.jpcc.4c06624
J. Phys. Chem. C XXXX, XXX, XXX−XXX

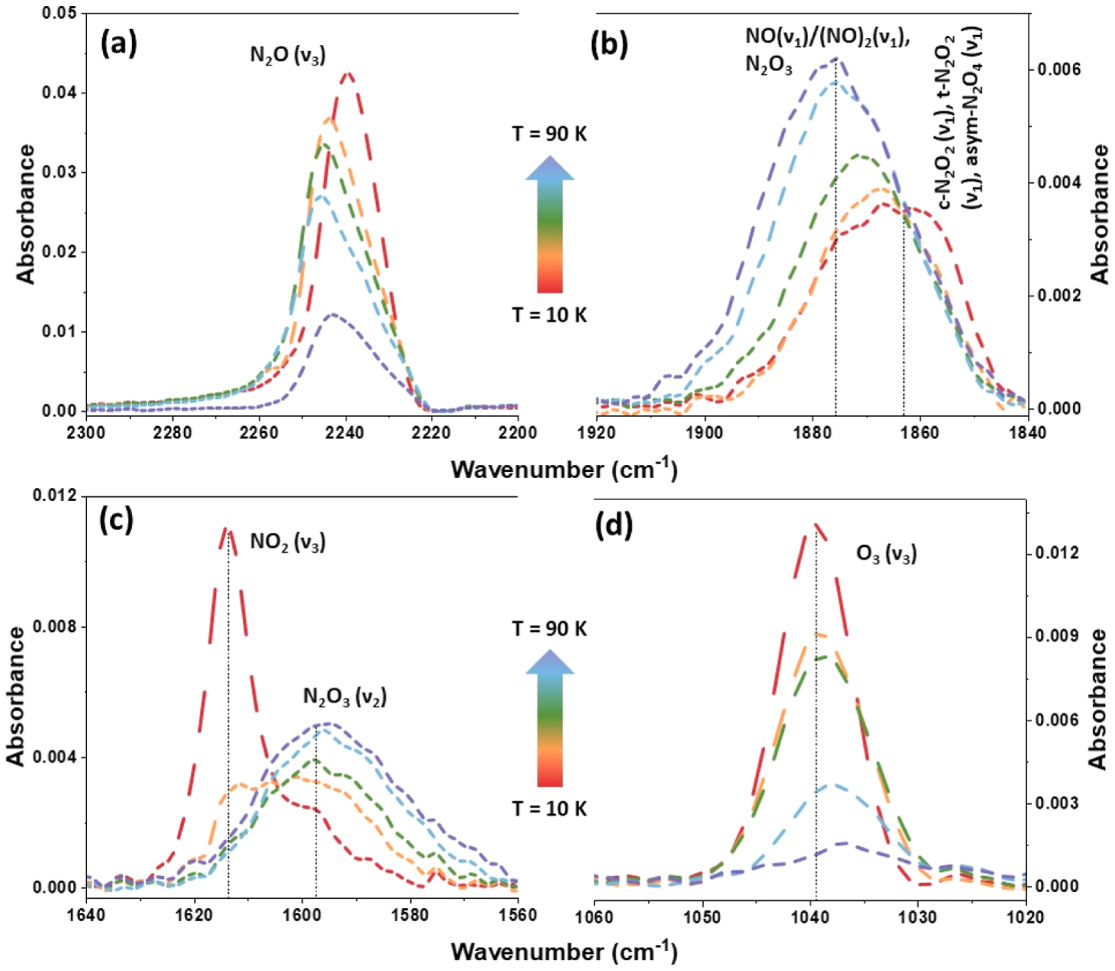

Figure 5. Temperature-dependent RAIR spectra of 4 h photoirradiated N_2O ice. Major IR bands are shown for N_2O, NO, NO_2, N_2O_2, N_2O_3, N_2O_4, O_3. 150 ML of N_2O ice was photoirradiated for 4 h, then annealed to 90 K with a heating rate of 2 K min^{-1}.

30 signal can be attributed to various photoinduced products such as NO_2, N_2O_5, N_2O_3, N_2O_2, and N_2O_4. This study provides valuable insights into the desorption behavior of photoproducts and their transition from solid to gaseous phase under cryogenic conditions.

Comparative Analysis of Radical Diffusion and Photoproduct Formation. At 10 K, the diffusion and mobility of the reactive intermediates are minimized, potentially arresting further reactions. To examine this theory, we annealed the 4 h photoirradiated sample to 90 K and collected temperature-dependent RAIR spectra (Figure 5). Interestingly, during thermal annealing of photoirradiated N_2O ice, we observed a significant increase in NO and N_2O_3 (Figure 5b,c) alongside a reduction in NO_2 and O_3 (Figure 5c,d). Additionally, a decrease in peak intensity in the ν_3 mode of N_2O was also observed (Figure 5a), which is attributed to the dissociation of N_2O by reacting with reactive diffused oxygen radicals (reaction paths 3, 4, 8, 9, and 14). Increase in the formation of more NO can be explained by the reaction path 3, where N_2O is combined with O to form two NO. Desorption of N_2O is unlikely here, as pure N_2O only starts desorbing after 80 K (Figure S5).

The increased formation of N_2O_3 molecules during thermal annealing of photoirradiated N_2O ice indicates a reaction pathway where NO_2 combines with O radicals. The availability of oxygen and NO radicals, which become mobile as the temperature increases, leads to more reaction products. Notably, we did not calculate the column density of any molecules because of the significant band overlap among N−O bond-bearing species. In the equation for calculating column density from band area, the band area and column density are directly proportional, assuming other factors remain constant.

To gain a deeper understanding of the trapping of photoproduced intermediates at 10 K and the subsequent increase in molecular mobility of radicals at higher temperatures, we carried out photoirradiation at 50 K. We calculated the abundance of photoproducts and compared them with those produced at 10 K (Figure 6). Figure S6 shows the time-dependent formation of photoproducts at 50 K. At this temperature, the abundance of NO_2 and O_3 is very low compared to the larger photoproducts such as N_2O_3, N_2O_5, *c*/*t*-N_2O_2, and N_2O_4 (Figure S6). The band area of photoproduced O_3, and NO_2 start to decrease after 50 min, while N_2O_2/N_2O_4 and N_2O_5 begin to decrease after 150 min while N_2O_3 band area does not decrease until 240 min (Figure S7). In the case of O_3, the reduced band area can be attributed to the desorption (Figure 4b) and dissociation followed by recombination with N_2O (reaction paths 9 and 14) in the ice matrix. A decrease in the band area of NO_2 after 50 min can be attributed to the dissociation of NO_2 and recombination with other molecules to produce secondary heavy molecules (reaction paths 12,13 and 14). Similarly, the decrease in the

https://doi.org/10.1021/acs.jpcc.4c06624
J. Phys. Chem. C XXXX, XXX, XXX−XXX

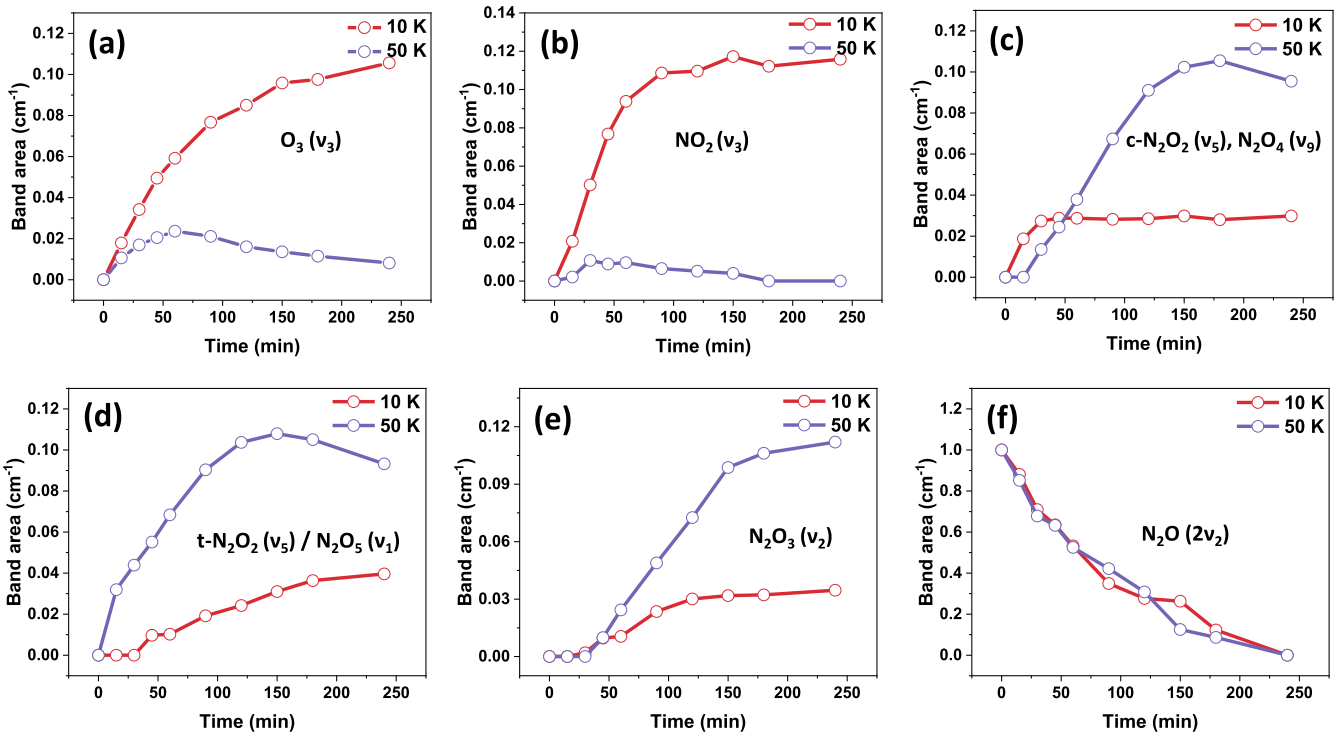

Figure 6. Integrated band areas versus VUV irradiation time for selected photoproducts at 10 and 50 K. The plots show: (a) O_3 (ν_3), (b) NO_2 (ν_3), (c) cis(*c*)-N_2O_2 (ν_5) and N_2O_4 (ν_9) and (d) trans (*t*)-N_2O_2 (ν_5), N_2O_5 (ν_1), (e) N_2O_3 (ν_2), and (f) N_2O ($2\nu_2$). For N_2O, the band areas are normalized for 10 and 50 K.

band area for N_2O_5 and N_2O_2/N_2O_4 can be attributed to dissociation due to intense VUV irradiation.

Figure 6 compares the abundance of photoproducts produced after 4 h of photoirradiation at 10 K, and 50 K. It shows that the earlier photoproducts, O_3 and NO_2 are relatively higher in abundance at 10 K, while the secondary photoproducts, N_2O_3, N_2O_2/N_2O_4, and N_2O_5 are more abundant at 50 K. This comparison clearly shows a selective difference in the photoproduct concentration at two different temperatures. Importantly, the crystalline nature of N_2O ice at 50 K (Figure S8) does not contribute to this selective photoproduct formation. To substantiate this, we conducted a control experiment in which N_2O ice was first crystallized by annealing it to 50 K. Subsequently the sample was cooled to 10 K, and irradiated for 4 h. The resulting photoproducts were similar to those observed at 10 K (Figure S9), clearly indicating that the hindered diffusion of radicals at lower temperatures limits the formation of secondary photoproducts. Thus, we conclude that the diffusion of reactive radicals at higher temperatures plays a key role in selectively enhancing the concentration of secondary photoproducts.

CONCLUSIONS

This study demonstrated that VUV photolysis of N_2O generates a range of photoproducts, including O_3, NO, NO_2, N_2O_2, N_2O_3, N_2O_4, and N_2O_5, which were characterized using RAIRS, SIMS and TPD-MS. Thermal annealing of the photoirradiated N_2O ice showed an increase in NO and N_2O_3 and a decrease in NO_2 and O_3, indicating that thermal diffusion of reactive intermediates, which are majorly reactive oxygen species (O and O_3) continue to drive the reactions. Experiments conducted at 10 and 50 K revealed that three atom photoproducts (O_3 and NO_2) dominate at 10 K, while four or more atom photoproducts (N_2O_2, N_2O_3, N_2O_4, and N_2O_5) are prevalent at 50 K. This behavior is attributed to the restricted diffusion of radicals at 10 K, which limits radical–radical reactions leading to primary products, whereas higher temperatures promote greater diffusion and recombination, leading to the formation of heavier photoproducts. These findings highlight the crucial role of diffusion restrictions and thermodynamic stability in the formation of photoproducts in icy matrices.

ASSOCIATED CONTENT

Supporting Information

The Supporting Information is available free of charge at https://pubs.acs.org/doi/10.1021/acs.jpcc.4c06624.

It includes temperature and time-dependent RAIR spectra and the emission spectrum of the model 634 Deuterium lamp (PDF)

AUTHOR INFORMATION

Corresponding Author

Thalappil Pradeep − *DST Unit of Nanoscience (DST UNS) and Thematic Unit of Excellence (TUE), Department of Chemistry, Indian Institute of Technology Madras, Chennai 600036, India; International Centre for Clean Water, IIT Madras Research Park, Chennai 600113, India;* orcid.org/0000-0003-3174-534X; Email: pradeep@iitm.ac.in

Authors

Bijesh K. Malla − *DST Unit of Nanoscience (DST UNS) and Thematic Unit of Excellence (TUE), Department of Chemistry, Indian Institute of Technology Madras, Chennai 600036, India*

https://doi.org/10.1021/acs.jpcc.4c06624
J. Phys. Chem. C XXXX, XXX, XXX−XXX

Soham Chowdhury − *DST Unit of Nanoscience (DST UNS) and Thematic Unit of Excellence (TUE), Department of Chemistry, Indian Institute of Technology Madras, Chennai 600036, India*

Devansh Paliwal − *DST Unit of Nanoscience (DST UNS) and Thematic Unit of Excellence (TUE), Department of Chemistry, Indian Institute of Technology Madras, Chennai 600036, India*

Hanoona K. M. − *Department of Chemistry, Mar Ivanios College, Thiruvananthapuram, Kerala 695015, India*

Gaurav Vishwakarma − *DST Unit of Nanoscience (DST UNS) and Thematic Unit of Excellence (TUE), Department of Chemistry, Indian Institute of Technology Madras, Chennai 600036, India;* orcid.org/0009-0002-6076-3299

Rabin Rajan J. Methikkalam − *Department of Chemistry, Mar Ivanios College, Thiruvananthapuram, Kerala 695015, India*

Complete contact information is available at: https://pubs.acs.org/10.1021/acs.jpcc.4c06624

Author Contributions

T.P. and B.K.M. designed the research. B.K.M., S.C., D.P., and H.K.M., have performed the experiments. T.P. supervised its progress. B.K.M. analyzed the results. The first draft of the manuscript was written by B.K.M. The final version of the manuscript was prepared, including the contributions of all authors.

Notes

The authors declare no competing financial interest.

■ ACKNOWLEDGMENTS

We acknowledge the Science and Engineering Research Board (SERB) for the Core Research grant (CRG/2018/003922), Department of Science and Technology (DST), and Government of India for research funding. T.P. acknowledges funding from the Centre of Excellence on Molecular Materials and Functions under the Institution of Eminence scheme of IIT Madras. B.K.M. thanks the Council of Scientific and Industrial Research (CSIR) for his research fellowship. S.C. thanks IITM for their research fellowship.

■ REFERENCES

(1) Öberg, K. I. Photochemistry and Astrochemistry: Photochemical Pathways to Interstellar Complex Organic Molecules. *Chem. Rev.* **2016**, *116* (17), 9631−9663.

(2) McGuire, B. A. Census of Interstellar, Circumstellar, Extragalactic, Protoplanetary Disk, and Exoplanetary Molecules. *Astrophys. J. Suppl. Ser.* **2022**, *259* (2), 30.

(3) Cami, J.; Bernard-Salas, J.; Peeters, E.; Malek, S. E. Detection of $C_{60}$and C_{70} in a Young Planetary Nebula. *Science* **2010**, *329* (5996), 1180−1182.

(4) Arumainayagam, C. R.; Garrod, R. T.; Boyer, M. C.; Hay, A. K.; Bao, S. T.; Campbell, J. S.; Wang, J.; Nowak, C. M.; Arumainayagam, M. R.; Hodge, P. J. Extraterrestrial Prebiotic Molecules: Photochemistry vs. Radiation Chemistry of Interstellar Ices. *Chem. Soc. Rev.* **2019**, *48* (8), 2293−2314.

(5) Singh, S. K.; Zhu, C.; La Jeunesse, J.; Fortenberry, R. C.; Kaiser, R. I. Experimental Identification of Aminomethanol (NH_2CH_2OH)—the Key Intermediate in the Strecker Synthesis. *Nat. Commun.* **2022**, *13* (1), 375−377.

(6) Schutte, W. A.; Allamandola, L. J.; Sandford, S. A. Formaldehyde and Organic Molecule Production in Astrophysical Ices at Cryogenic Temperatures. *Science* **1993**, *259* (5098), 1143−1145.

(7) Malla, B. K.; Vishwakarma, G.; Chowdhury, S.; Pradeep, T. Vacuum Ultraviolet Photolysis of Condensed Methyl Chloride in Interstellar Model Conditions and Trapping of Intermediates at Intergrain Interfaces. *J. Phys. Chem. C* **2023**, *127* (50), 24149−24157.

(8) Cuppen, H. M.; Karssemeijer, L. J.; Lamberts, T. The Kinetic Monte Carlo Method as a Way to Solve the Master Equation for Interstellar Grain Chemistry. *Chem. Rev.* **2013**, *113* (12), 8840−8871.

(9) Noble, J. A.; Michoulier, E.; Aupetit, C.; Mascetti, J. Influence of Ice Structure on the Soft UV Photochemistry of PAHs Embedded in Solid Water. *Astron. Astrophys.* **2020**, *644*, A22.

(10) Lilach, Y.; Asscher, M. Photochemistry of Caged Molecules: CD_3Cl@Ice. *J. Chem. Phys.* **2003**, *119* (1), 407−412.

(11) Asscher, Y. A. and M. Water at Interfaces. *Phys. Chem. Chem. Phys.* **2008**, *10* (32), 4676.

(12) Laffon, C.; Lasne, J.; Bournel, F.; Schulte, K.; Lacombe, S.; Parent, P. Photochemistry of Carbon Monoxide and Methanol in Water and Nitric Acid Hydrate Ices: A NEXAFS Study. *Phys. Chem. Chem. Phys.* **2010**, *12* (36), 10865−10870.

(13) Ramakrishnan, S.; Sagi, R.; Mahapatra, N.; Asscher, M. Effect of Coadsorbed Oxygen on the Photochemistry of Methane Embedded in Amorphous Solid Water. *J. Phys. Chem. C* **2018**, *122* (27), 15287−15296.

(14) Schriver, A.; Coanga, J. M.; Schriver-Mazzuoli, L.; Ehrenfreund, P. Vibrational Spectra and UV Photochemistry of $(CH_2)_2O$ Thin Films and $(CH_2)_2O$ in Amorphous Water Ice. *Chem. Phys.* **2004**, *303* (1−2), 13−25.

(15) Yabushita, A.; Hama, T.; Kawasaki, M. Photochemical Reaction Processes during Vacuum-Ultraviolet Irradiation of Water Ice. *J. Photochem. Photobiol. C Photochem. Rev.* **2013**, *16*, 46−61.

(16) Kulikov, M. Y.; Feigin, A. M.; Schrems, O. H_2O_2 Photoproduction inside H_2O and H_2O:O_2 Ices at 20−140 K. *Sci. Rep.* **2019**, *9* (1), 11375−11379.

(17) Ziurys, L. M.; Apponi, A. J.; Hollis, J. M.; Snyder, L. E. Detection of Interstellar N_2O: A New Molecule Containing an N-O Bond. *Astrophys. J.* **1994**, *436* (september 2016), L181.

(18) Nazari, P.; Rocha, W. R. M.; Rubinstein, A. E.; Slavicinska, K.; Rachid, M. G.; Van Dishoeck, E. F.; Megeath, S. T.; Gutermuth, R.; Tyagi, H.; Brunken, N.; et al. Hunting for Complex Cyanides in Protostellar Ices with the JWST - A Tentative Detection of CH3CN and C_2H_5CN. *Astron. Astrophys.* **2024**, *686*, A71.

(19) Tsai, W.-T.; Fernando, J.; Gomes, P. Fate of Chloromethanes in the Atmospheric Environment: Implications for Human Health, Ozone Formation and Depletion, and Global Warming Impacts. *Toxics* **2017**, *5* (4), 23.

(20) Sivaraman, B.; Ptasinska, S.; Jheeta, S.; Mason, N. J. Electron Irradiation of Solid Nitrous Oxide. *Chem. Phys. Lett.* **2008**, *460* (1−3), 108−111.

(21) Knauth, D. C.; Andersson, B. G.; McCandliss, S. R.; Warren Moos, H. The Interstellar N_2 Abundance towards HD 124314 from Far-Ultraviolet Observations. *Nat.* **2004**, *429* (6992), 636−638.

(22) Larsson, B.; Liseau, R.; Pagani, L.; Bergman, P.; Bernath, P.; Biver, N.; Black, J. H.; Booth, R. S.; Buat, V.; Crovisier, J.; et al. Molecular oxygen in the ρ Ophiuchi cloud. *Astron. Astrophys.* **2007**, *466* (3), 999−1003.

(23) Goldsmith, P. F.; Liseau, R.; Bell, T. A.; Black, J. H.; Chen, J. H.; Hollenbach, D.; Kaufman, M. J.; Li, D.; Lis, D. C.; Melnick, G.; et al. Herschel measurements of molecular oxygen in Orion. *Astrophys. J.* **2011**, *737* (2), 96.

(24) Snyder, L. E.; Kuan, Y.-J.; Ziurys, L. M.; Hollis, J. M.; Snyder, L. E.; Kuan, Y.-J.; Ziurys, L. M.; Hollis, J. M. New 3 Millimeter Observations of Interstellar HNO: Reinstating a Discredited Identification. *ApJL* **1993**, *403*, L17.

(25) Ziurys, L. M.; Apponi, A. J.; Hollis, J. M.; Snyder, L. E.; Ziurys, L. M.; Apponi, A. J.; Hollis, J. M.; Snyder, L. E. Detection of Interstellar N 2O: A New Molecule Containing an N-O Bond. *ApJL* **1994**, *436*, L181.

(26) Coutens, A.; Ligterink, N. F. W.; Loison, J. C.; Wakelam, V.; Calcutt, H.; Drozdovskaya, M. N.; Jørgensen, J. K.; Müller, H. S. P.; Van Dishoeck, E. F.; Wampfler, S. F. The ALMA-PILS Survey: First

Detection of Nitrous Acid (HONO) in the Interstellar Medium. *Astron. Astrophys.* **2019**, *623*, L13.
(27) Marcelino, N.; Cernicharo, J.; Tercero, B.; Roueff, E. Discovery of Fulminic Acid, HCNO, in Dark Clouds. *ApJL* **2009**, *690* (1), L27−L30.
(28) Liszt, H. S.; Turner, B. E.; Liszt, H. S.; Turner, B. E. Microwave Detection of Interstellar NO. *ApJL* **1978**, *224*, L73−L76.
(29) Rivilla, V. M.; Martín-Pintado, J.; Jiménez-Serra, I.; Martín, S.; Rodríguez-Almeida, L. F.; Requena-Torres, M. A.; Rico-Villas, F.; Zeng, S.; Briones, C. Prebiotic Precursors of the Primordial RNA World in Space: Detection of NH $_2$ OH. *Astrophys. J. Lett.* **2020**, *899* (2), L28.
(30) Jamieson, C. S.; Bennett, C. J.; Mebel, A. M.; Kaiser, R. I. Investigating the Mechanism for the Formation of Nitrous Oxide [N $_2$ O(X 1 Σ +)] in Extraterrestrial Ices. *Astrophys. J.* **2005**, *624* (1), 436−447.
(31) Halfen, D. T.; Apponi, A. J.; Ziurys, L. M. Evaluating the N/O Chemical Network: The Distribution of N $_2$ O and NO in the Sagittarius B2 Complex. *Astrophys. J.* **2001**, *561* (1), 244−253.
(32) Almeida, G. C.; Pilling, S.; de Barros, A. L. F.; da Costa, C. A. P.; Pereira, R. C.; da Silveira, E. F. Processing of N_2O Ice by Fast Ions: Implications on Nitrogen Chemistry in Cold Astrophysical Environments. *Mon. Not. R. Astron. Soc.* **2017**, *471* (2), 1330−1340.
(33) Bag, S.; Bhuin, R. G.; Methikkalam, R. R. J.; Pradeep, T.; Kephart, L.; Walker, J.; Kuchta, K.; Martin, D.; Wei, J. Development of Ultralow Energy (1−10 EV) Ion Scattering Spectrometry Coupled with Reflection Absorption Infrared Spectroscopy and Temperature Programmed Desorption for the Investigation of Molecular Solids. *Rev. Sci. Instrum.* **2014**, *85* (1), 1−7.
(34) Malla, B. K.; Vishwakarma, G.; Chowdhury, S.; Nayak, S. K.; Yamijala, S. S. R. K. C.; Pradeep, T. Formation and Dissociation of Dimethyl Ether Clathrate Hydrate in Interstellar Ice Mimics. *J. Phys. Chem. C* **2024**, *128* (6), 2463−2470.
(35) Malla, B. K.; Vishwakarma, G.; Chowdhury, S.; Selvarajan, P.; Pradeep, T. Formation of Ethane Clathrate Hydrate in Ultrahigh Vacuum by Thermal Annealing. *J. Phys. Chem. C* **2022**, *126* (42), 17983−17989.
(36) Vishwakarma, G.; Malla, B. K.; Kumar, R.; Pradeep, T. Partitioning Photochemically Formed CO 2 into Clathrate Hydrate under Interstellar Conditions. *Phys. Chem. Chem. Phys.* **2024**, *26* (22), 16008−16016.
(37) Kang, H. Chemistry of Ice Surfaces. Elementary Reaction Steps on Ice Studied by Reactive Ion Scattering. *Acc. Chem. Res.* **2005**, *38* (12), 893−900.
(38) Hahn, J. R.; Lee, C. W.; Han, S. J.; Lahaye, R. J. W. E.; Kang, H. Low-Energy Cs^+ Scattering from Water on Pt(111): A Kinetic Energy Analysis of the Cs^+-Water Clusters. *J. Phys. Chem. A* **2002**, *106* (42), 9827−9831.
(39) Cyriac, J.; Pradeep, T.; Kang, H.; Souda, R.; Cooks, R. G. Low-Energy Ionic Collisions at Molecular Solids. *Chem. Soc. Rev.* **2012**, *112*, 5356−5411.
(40) Bartmess, J. E.; Georgiadis, R. M. Empirical Methods for Determination of Ionization Gauge Relative Sensitivities for Different Gases. *Vacuum* **1983**, *33* (3), 149−153.
(41) Vishwakarma, G.; Malla, B. K.; Chowdhury, S.; Khandare, S. P.; Pradeep, T. Existence of Acetaldehyde Clathrate Hydrate and Its Dissociation Leading to Cubic Ice under Ultrahigh Vacuum and Cryogenic Conditions. *J. Phys. Chem. Lett.* **2023**, *14*, 5328−5334.
(42) Lee, D. H.; Kang, H. Acid-Promoted Crystallization of Amorphous Solid Water. *J. Phys. Chem. C* **2018**, *122* (42), 24164−24170.
(43) Mokrane, H.; Chaabouni, H.; Accolla, M.; Congiu, E.; Dulieu, F.; Chehrouri, M.; Lemaire, J. L. Experimental Evidence for Water Formation via Ozone Hydrogenation on Dust Grains at 10 K. *Astrophys. J.* **2009**, *705* (2), L195.
(44) Hisatsune, I. C.; Devlin, J. P.; Wada, Y. Infrared Spectra of Some Unstable Isomers of N_2O_4 and N_2O_3. *J. Chem. Phys.* **1960**, *33* (3), 714−719.
(45) Fulvio, D.; Baratta, G. A.; Sivaraman, B.; Mason, N. J.; da Silveira, E. F.; de Barros, A. L. F.; Pandoli, O.; Strazzulla, G.; Palumbo, M. E. Ion Irradiation of N_2O Ices and NO_2:N_2O_4 Ice Mixtures: First Steps to Understand the Evolution of Molecules with the N−O Bond in Space. *Mon. Not. R. Astron. Soc.* **2018**, *483* (1), 381−391.
(46) Hisatsune, I. C.; Devlin, J. P. Existence of N_2O_4 Isomers. *J. Chem. Phys.* **1959**, *31* (4), 1130−1131.
(47) Hudson, R. L.; Loeffler, M. J.; Gerakines, P. A. Infrared Spectra and Band Strengths of Amorphous and Crystalline N2O. *J. Chem. Phys.* **2017**, *146* (2), 24304.
(48) Gimmler, G.; Havenith, M. High-Resolution IR Spectroscopy of the N_2O−H_2O and N_2O−D_2O van Der Waals Complexes. *J. Mol. Spectrosc.* **2002**, *216* (2), 315−321.
(49) Zelikoff, M.; Aschenbrand, L. M. Vacuum Ultraviolet Photochemistry, Part I. Nitrous Oxide at 1470 A. *J. Chem. Phys.* **1954**, *22* (10), 1680−1684.
(50) Peyerimhoff, S. D.; Buenker, R. J. Theoretical Study of the Geometry and Spectrum of Nitrous Oxide. *J. Chem. Phys.* **1968**, *49* (6), 2473−2487.
(51) Ellison, G. B. Chemistry of Atmospheres: An Introduction to the Chemistry of the Atmospheres of Earth, the Planets, and Their Satellites, 3rd Edition (Wayne, Richard P.). *J. Chem. Educ.* **2003**, *80* (3), 264.
(52) Minissale, M.; Fedoseev, G.; Congiu, E.; Ioppolo, S.; Dulieu, F.; Linnartz, H. Solid State Chemistry of Nitrogen Oxides − Part I: Surface Consumption of NO. *Phys. Chem. Chem. Phys.* **2014**, *16* (18), 8257−8269.
(53) Jo, S. K.; Kiss, J.; Castro, M. E.; White, J. M. Mass Effects in Photodissociation of Chloromethane. *J Am Chem Soc* **1992**, *482*, 310−315.
(54) Gilton, T. L.; Dehnbostel, C. P.; Cowin, J. P. Electron Transmission through Layers of H_2O and Xe in the Ultrahigh Vacuum Photoreduction of CH3Cl on Ni(111). *J. Chem. Phys.* **1989**, *91* (3), 1937−1938.
(55) Jo, S. K.; White, J. M. Low Energy (<1 EV) Electron Transmission through Condensed Layers of Water. *J. Chem. Phys.* **1991**, *94* (8), 5761−5764.
(56) Nagesha, K.; Fabrikant, I. I.; Sanche, L. Electron Attachment to CF_3Cl and CH_3Cl on the Surface and in the Bulk of Solid Kr. *J. Chem. Phys.* **2001**, *114* (11), 4934−4944.

https://doi.org/10.1021/acs.jpcc.4c06624
J. Phys. Chem. C XXXX, XXX, XXX−XXX